Dc Electrical Breakdown of Liquid Nitrogen under Simulated Quench State in Pool Cooled High Tc Superconducting Power Apparatus Pt. 1. Analytical Study of Bubble Behavior

Hara, Masanori
Department of Electrical and Electronic Systems Engineering, Kyushu University : Professor

Wang, Zhen-Chao
Department of Electrical and Electronic Systems Engineering, Kyushu University : Graduate Student (At present, Eiritu Electronics Industry Co.)

Matsuura, Shunsuke
Department of Electrical and Electronic Systems Engineering, Kyushu University : Graduate Student

Takano, Koji
Department of Electrical and Electronic Systems Engineering, Kyushu University : Graduate Student

https://doi.org/10.15017/1498314

出版情報：九州大学大学院システム情報科学紀要. 3 (1), pp.23-33, 1997-12-22. Faculty of Information Science and Electrical Engineering, Kyushu University
バージョン：
権利関係：

九州大学大学院
システム情報科学研究科報告
第3巻　第1号　平成10年3月

Research Reports on Information Science and
Electrical Engineering of Kyushu University
Vol. 3, No. 1, March 1998

Dc Electrical Breakdown of Liquid Nitrogen under Simulated Quench State in Pool Cooled High T_C Superconducting Power Apparatus

Pt. 1. Analytical Study of Bubble Behavior

Masanori HARA*, Zhen-Chao WANG**, Shunsuke MATSUURA***
and Koji TAKANO***

(Received December 22, 1997)

Abstract: The present paper consists of two parts. In the Part 1 thermal bubble behavior in liquid nitrogen under dc non-uniform fields that will take part in electrical breakdown in high T_C superconducting power apparatus at quenching conditions is dealt with theoretically. The results show that electrical gradient force affects severely bubble motion and causes bubble coalescence in the gap and that Maxwell stress acting on the bubble surface changes the manner by which the bubble is released from a groove between fins on an electrode. The change in the bubble motion and boiling phenomena by non-uniform electric field will result in different breakdown behavior from that in a uniform field gap, and the choice of desired fin shape will minimize bubble effects on the breakdown voltage with finned electrode.

Keywords: Electrical breakdown, Superconducting coil, Fault current limiter, Quench, Boiling, Bubble, Liquid nitrogen, Gradient force

1. Introduction

Recent advances in high T_C superconductors have, during the past few years, stimulated increasing interest on high T_C superconducting (s.c.) power apparatus. The most economical coolant will be liquid nitrogen, which has been claimed long ago to be an excellent insulating fluid. At the quenching state of pool boiling nitrogen cooled s.c. power apparatus such as coils and fault current limiters, high electric field and thermal bubbles appear simultaneously in liquid nitrogen around a hot spot region and cause electrical breakdown there. With respect to this problem, Hara et al. have already studied bubble behavior and breakdown characteristics with a uniform field gap[1)-5)] and found breakdown is categorized into three mechanisms: 1) with a fast rising voltage in the order of 10kV/μs, no bubble deformation occurs until breakdown, and then the breakdown appears in the composite insulation system of undeformed bubbles and surrounding liquid,; 2) with a medium ramp voltage of the order of 10kV/ms, a large suspended bubble is elongated in which a spark is triggered; and 3) with slower ramp voltage in the order of 0.1kV/ms, boiling turns from nucleate boiling to film boiling at an earlier stage and a bubble fixed on a heater surface grows and bridges the gap before breakdown. Moreover, effects of non-uniform electric field on such a bubble motion were studied by them. Okubo et al. reported a relationship between transient breakdown voltage and boiling activity under approximately real s.c. coil operations and discussed the volume effect on the breakdown voltage[6)].

In the present report, bubble behavior and breakdown mechanism with dc non-uniform field gaps in liquid nitrogen are described systematically including a part of results obtained in the previous studies for a limited short gap[7)-8)].

The studied gap is a cylinder-to-plane gap, and cylinder surface is grooved circularly or longitudinally to find the fin effect on bubble-triggered breakdown mechanism. A heater is mounted in the cylinder to simulate a hot spot by quench of superconductor. Bubble behavior is studied both analytically and experimentally and measured breakdown characteristics are discussed on the basis of the bubble behavior. The results show that electric field affects not only the motion of suspended bubble but also the mechanism of bubble generation, such as the number of active boiling nuclei, bubble diameter, and release of bubble into the gap space from the groove, and that breakdown voltage characteristics depend on the

* Department of Electrical and Electronic Systems Engineering
** Department of Electrical and Electronic Systems Engineering, Graduate Student (At present, Eiritu Electronics Industry Co.)
*** Department of Electrical and Electronic Systems Engineering, Graduate Student

bubble behavior.

The results obtained are reported by dividing them into two parts: the Part 1 is the analytical study of bubble behavior and the Part 2[9] the experimental study on bubble behavior and bubble-triggered breakdown characteristics.

2. Electrode System and Electric Field

In pool cooling s.c. coils, fins on the wire surface are often made to improve the heat transfer from the wire to the surrounding liquid. Non-uniform electric fields will be formed between coil turns or coil layers when the quench occurs in them. In the present work, the non-uniform field was simulated by using a plane-to-cylinder electrode system as shown in **Fig. 1**(a). On the cylinder surface, circular or longitudinal triangular fins as shown in **Fig. 1**(b) were made to find the effect of fin orientation on bubble behavior.

Each electrode system was denoted as CS, CC or CL system and the coordinates were given as (x, y) in the gap space and (R, θ) on the cylinder as shown in **Figs. 1**(a) and (c). To know the combined effect of electrical gradient and gravitational forces on bubble motion, four arrangements of electrode system, as shown in **Fig. 1**(c), were studied and were denoted as I, II, III, and IV. For example, a gap with smooth cylinder and arrangement III was denoted as the electrode system CS-III.

Fin pitch and height are 0.5mm and $0.25\sqrt{3}$ mm, respectively. Considering practical large s.c. coils and fault current limiters, cylinder diameter is taken as 10mm and gap length is changed within 0.5-40mm in the theoretical study.

The electric field in the studied gap can be divided into two components for the field calculation: a macroscopic non-uniform field produced by the smooth electrode and a microscopic non-uniform field due to the fin. The former component $\boldsymbol{E}$ was given by a plane-to-cylinder gap and calculated according to equations (1) and (2).

$$E_x=\frac{N}{2\pi\varepsilon_l}\left\{\frac{\sqrt{D^2-R^2}+x}{(\sqrt{D^2-R^2}+x)^2+y^2}+\frac{\sqrt{D^2-R^2}-x}{(\sqrt{D^2-R^2}-x)^2+y^2}\right\},$$

$$E_y=\frac{N}{2\pi\varepsilon_l}\left\{\frac{y}{(\sqrt{D^2-R^2}+x)^2+y^2}+\frac{y}{(\sqrt{D^2-R^2}-x)^2+y^2}\right\}, \quad (1)$$

where ε_l is the dielectric permittivity of liquid nitrogen and

$$N=\frac{2\pi\varepsilon_l V_a}{\ln\{(D-R+\sqrt{D^2-R^2})/(R-D+\sqrt{D^2+R^2})\}}. \quad (2)$$

The magnitude of the microscopic non-uniform field was obtained as the product of an external electric field $\boldsymbol{E}$ and a field enhancement factor k to account for the effect of the fins. The value of k was calculated numerically by the finite element method for a hatched cell in a parallel plane gap, as shown in **Fig. 2**(a), where one of planes has triangular fins.

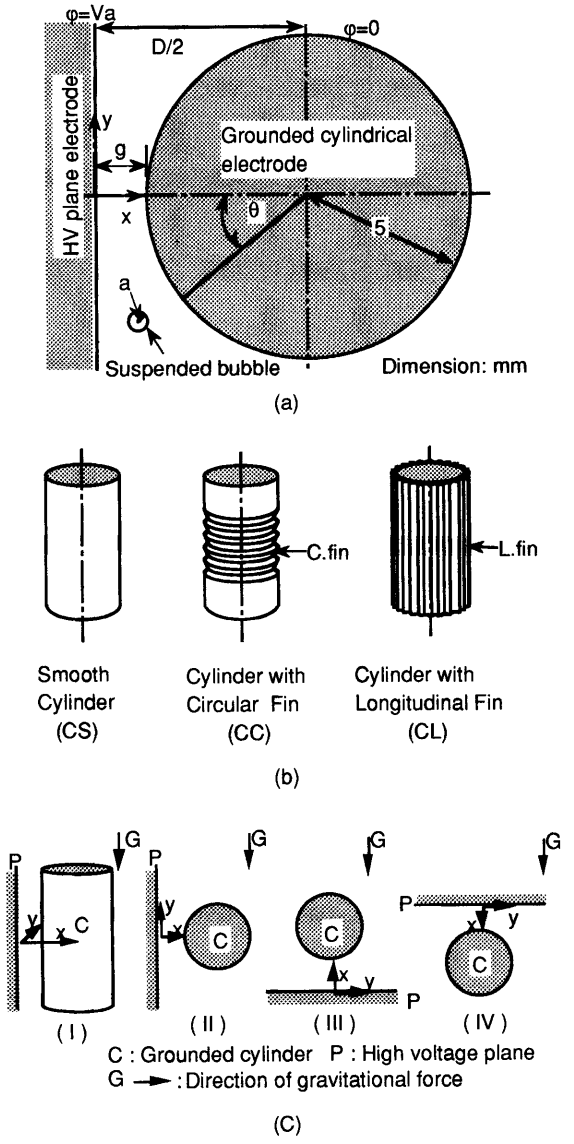

Fig. 1 Studied electrodes
(a) Electrode system and coordinates for analysis of bubble motion,
(b) Surface condition of cylindrical electrode,
(c) Arrangement of electrode system.

The calculated k along the line through the top or bottom of the groove is illustrated in **Fig. 2**(b). Clearly, the field enhancement factor increases drastically near the fin tip, but decreases down to zero upon reaching the groove bottom between fins.

3. Assumptions and Forces Acting on Bubbles

Bubble behavior is analyzed in two categories: bubbles suspended in the gap and those trapped in the groove between fins. The applied voltage V_a is dc and is varied within a range of zero to breakdown voltage which was estimated according to an empirical formula for liquid nitrogen or the streamer theory for nitrogen gas as will be described later.

3.1 Assumptions for the analysis

For simplicity of the analysis, the following are assumed:

1) liquid motion by the electrostriction and volume force, such as Coulomb force on charge contained in liquid, are negligible;

2) the shape of suspended bubble is spherical, and its radius a is relatively small compared to the gap length g;

3) force acting on a suspended bubble consists of gradient force, drag force and buoyancy, and the net charge on the bubble is negligibly small;

4) a bubble is released from the cylinder surface with zero initial velocity;

5) bubbles collide elastically with the electrode; and

6) coefficient of friction between bubble and electrode is zero when the bubble slips along the electrode surface.

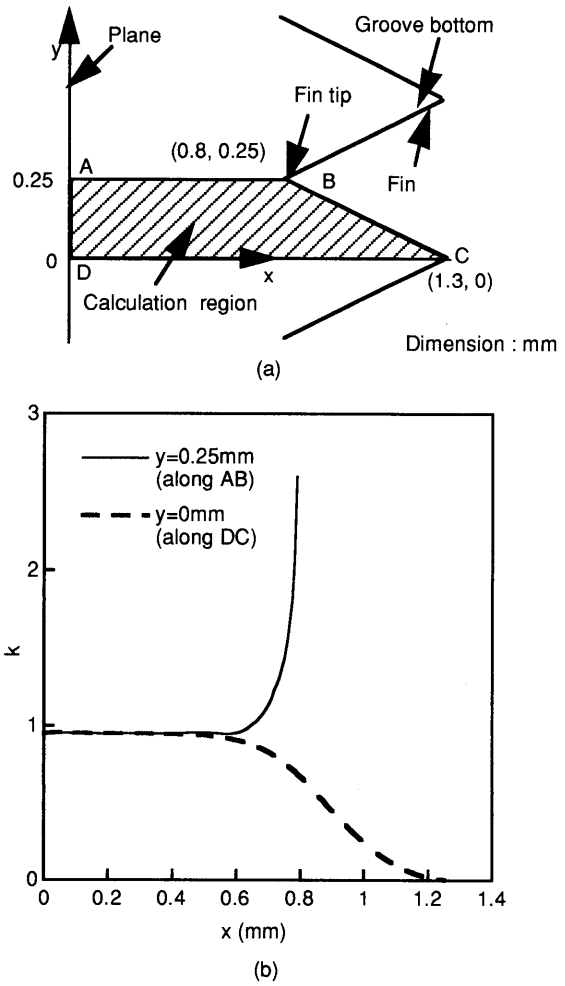

Fig. 2 Fin shape and field enhancement factor near a fin
(a) Fin shape and notation for field calculation region,
(b) Field enhancement factor.

3.2 Forces acting on the bubbles

Before the analysis of bubble behavior, the forces acting on the bubble are summarized here. The force consists of drag force $\boldsymbol{F}_d$, buoyancy $\boldsymbol{F}_B$, and electrical gradient force $\boldsymbol{F}_g$ for a suspended bubble, and Maxwell stress $\boldsymbol{P}_e$, surface tension $\boldsymbol{P}_\sigma$, hydraulic pressure $\boldsymbol{P}_S$ and gas pressure $\boldsymbol{P}_V$ on the surface of trapped bubble in the groove, as shown in **Fig. 3**. The properties of saturated nitrogen at 1 atm. required for numerical calculation of forces are given in **Table 1**.

(1) Drag force

As the viscosity of the gas in the bubble is neglected, the drag force in the stationary liquid nitrogen is given by

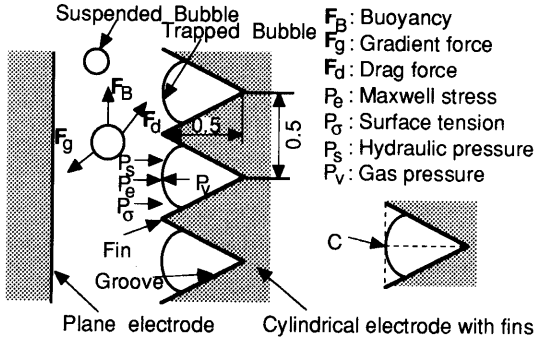

Fig. 3 Fin shape and forces acting on bubbles.

Table 1 Properties of saturated nitrogen at 1 atm.

ρ_l(kg/m³)	ρ_g(kg/m³)	$\varepsilon_l/\varepsilon_0$	$\varepsilon_g/\varepsilon_0-1$	η(μPa-s)
824.2	4.98	1.4318	5.87×10^{-4}	217

$$\boldsymbol{F}_d = -4\pi\eta a\boldsymbol{V}, \tag{3}$$

where η is the dynamic viscosity of liquid nitrogen and $\boldsymbol{V}$ the bubble velocity.

(2) Buoyancy

$$\boldsymbol{F}_B = \frac{4}{3}\pi a^3(\rho_l - \rho_g)\boldsymbol{G}, \tag{4}$$

where ρ_l is the density of liquid nitrogen, ρ_g the gas density inside the bubble, and $\boldsymbol{G}$ the gravitational acceleration.

(3) Gradient force

As well known, the gradient force on the spherical gas bubble is given by

$$\boldsymbol{F}_g = 2\pi a^3 \frac{\varepsilon_l(\varepsilon_g - \varepsilon_l)}{2\varepsilon_l + \varepsilon_g}\nabla\boldsymbol{E}^2, \tag{5}$$

where ε_g is the dielectric permittivity of gas inside the bubble, and $\boldsymbol{E}$ the external electric field at the bubble center.

In order to find the outline of gradient force, the direction and magnitude of gradient force on the unit bubble volume in the smooth cylinder-to-plane gap with g=0.8mm and R=5mm are calculated numerically. Calculation results are illustrated in **Figs. 4** and **5** in which v_b is bubble volume. From the observation of these figures, the following are recognized.

1) With smooth cylinder, the gradient force is maximum on the cylinder at the shortest gap and becomes extremely small near the plane electrode.

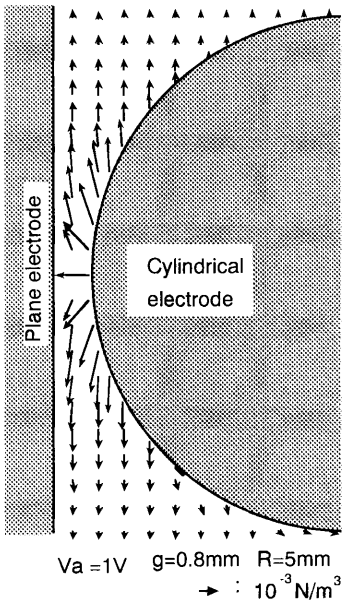

Fig. 4 Distribution of gradient force in a smooth cylinder-to-plane gap.

2) The gradient force can become much larger than the buoyancy at the breakdown voltage of the studied liquid gap, about 23kV.

3) The stagnation line on which the gradient force balances with buoyancy can appear before breakdown, and its position and shape depend on the orientation of electrode system with respect to the gravitational force.

4) Direction of gradient force changes with the position and bubbles are impelled into the region of lower electric field.

With the finned cylinder, the calculated gradient force is illustrated in **Figs. 6** and **7**, and the following are recognized.

1) The y component of gradient force directs to the plane electrode near the fin tip, while it turns towards

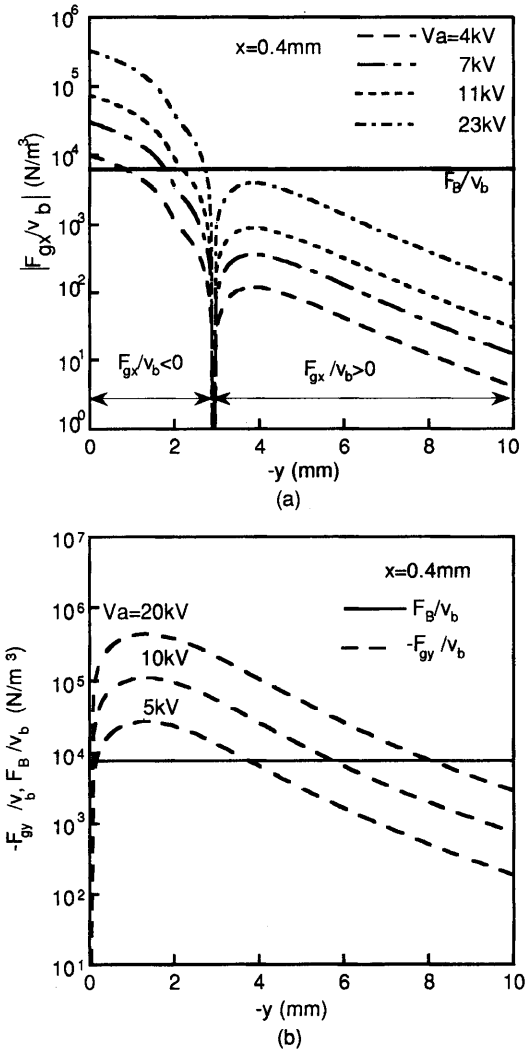

Fig. 5 Macroscopic gradient force as a function of y for x=0.4mm in **Fig. 1**(a) and g=0.8mm
(a) $\boldsymbol{F}_{gx}$ vs. y,
(b) $\boldsymbol{F}_{gy}$ vs. y.

the groove bottom in the space between fins, as shown in **Fig. 6**.

2) The gradient force near the fin tip reaches 10^3 times larger than buoyancy but remarkably drops in the groove bottom, as seen in **Fig. 7**. This means that the bubbles near the cylinder surface are either blown away from the fin tip or trapped in the groove easily. Therefore, no suspended bubbles will exist around the fin tip in the shortest gap region.

(4) Maxwell stress

Maxwell stress is perpendicular to the bubble surface and acts on the bubble radially inward. If $\boldsymbol{E}_{gt}$ $(=\boldsymbol{E}_{lt}=\boldsymbol{E})$ and $\boldsymbol{E}_{gn}$ $(=\boldsymbol{D}/\varepsilon_g)$ are, respectively, the tangential and normal components of electric field at a given point on the bubble inside surface, the corresponding Maxwell stresses at the point are given by

$$\boldsymbol{P}_{ep}=\frac{(\varepsilon_l-\varepsilon_g)\boldsymbol{E}^2}{2}, \tag{6}$$

and

$$\boldsymbol{P}_{en}=\frac{\boldsymbol{D}^2}{2}\left(\frac{1}{\varepsilon_g}-\frac{1}{\varepsilon_l}\right), \tag{7}$$

where $\boldsymbol{E}_g$ and $\boldsymbol{E}_l$ are electric fields at the inside and outside of bubble surface, respectively.

In order to calculate Maxwell stress on the surface of a bubble trapped in the groove, the bubble shape should be determined in advance. However, it depends on the stress. Then the stress at the surface point on the CD in **Fig. 2**(a) is calculated because the electric field at the point C in **Fig. 3** is always perpendicular to the bubble surface and Eqn.(7) is valid.

The calculated results for the circular finned cylinder are shown in **Fig. 8**. The Maxwell stress drops drastically with the x when the applied voltage is large enough to trap the bubble into the groove. This means that the shape of trapped bubble is almost independent of the applied voltage when the applied voltage increases beyond a critical value. That is, the bubble is released from the groove below the critical external electric field; but above it the surface of trapped bubble will exist near the x, giving a large drop in $\boldsymbol{P}_e$, as can be seen in **Fig. 8**(a). The $\boldsymbol{P}_e$ corresponding to the critical electric field will be discussed in section 3.2 of the Part 2.

The stress at the position C in **Fig. 3** decreases by one order or more with increasing value of θ, from 0 to 45°, as shown in **Fig. 8**(b).

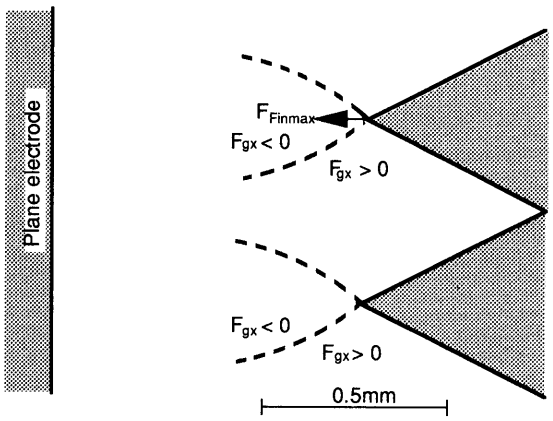

Fig. 6 Theoretically estimated boundary with respect to the direction of gradient force near the fin.

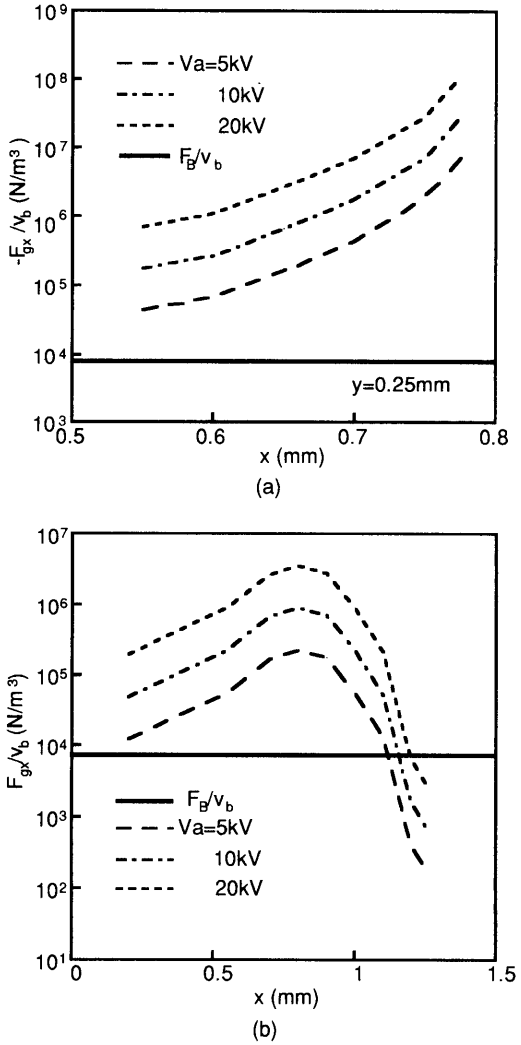

Fig. 7 Microscopic gradient force as a function of x in **Fig. 2**(a)
(a) Microscopic gradient force along the line of AB in **Fig. 2**(a),
(b) Microscopic gradient force along the line of DC in **Fig. 2**(a).

(5) Surface tension and others

Pressure by surface tension is given as

$$P_\sigma = \sigma\left(\frac{1}{r_1}+\frac{1}{r_2}\right) \tag{8}$$

where r_1 and r_2 are the principal radii of the curvature at a specific point on the bubble surface and σ the surface tension.

P_σ, P_s and P_v will be discussed in section 4.2 of Part 1 and in section 3.2 of Part 2 in this work, but is of little concern here.

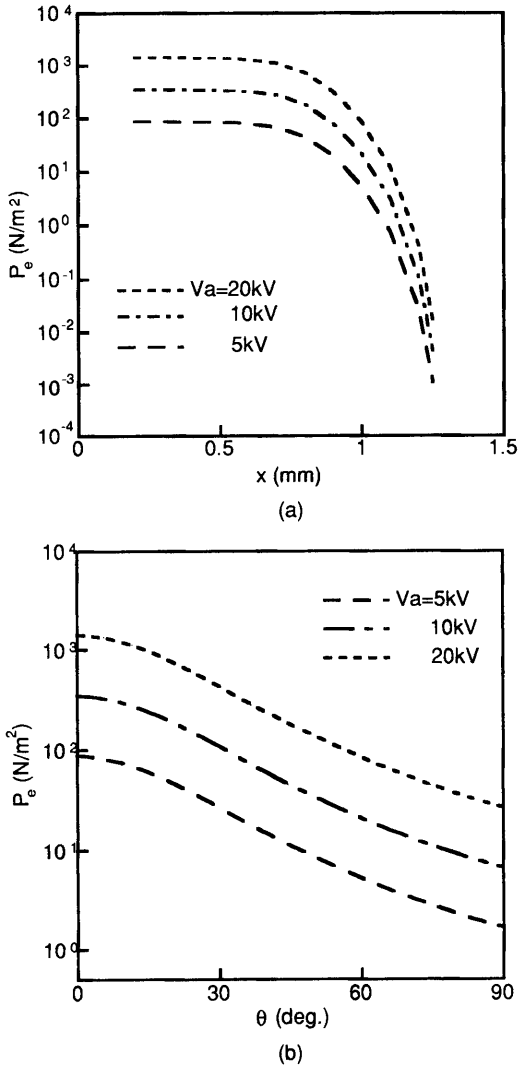

Fig. 8 Maxwell stress acting at the point C on surface of bubble trapped in the groove shown in **Fig. 3**
(a) P_e vs. x,
(b) P_e vs. θ.

4. Behavior of Suspended Bubble

4.1 Fundamental Equations of Bubble Motion

A suspended bubble affected by gradient force F_g, drag force F_d, and buoyancy F_B stated above will move according to the following equation; since the convection of liquid nitrogen was neglected,

$$M_{eff}\frac{dV}{dt} = 2\pi a^3 \frac{\varepsilon_l(\varepsilon_g-\varepsilon_l)}{2\varepsilon_l+\varepsilon^o}\nabla E^2 - 4\pi a\eta V + \frac{4\pi a^3}{3}\left(\rho_l-\rho_g\right)G, \tag{9}$$

where M_{eff} is the effective mass of the bubble in motion and given by[10]

$$M_{eff} = \frac{4}{3}\pi a^3\left(\rho_g+\frac{1}{2}\rho_l\right). \tag{10}$$

4.2 Bubble Motion in Smooth Cylinder-to-Plane Gap

In order to calculate bubble trajectory, velocity, and traveling time, the bubble radius, gap length, and applied voltage should be given as a premise. The bubble radius was taken as 0.04-0.32mm on the basis of our preliminary experiments and the maximum applicable voltage in the presence of thermal bubbles for the studied gap lengths of 0.5-40mm is considered to be in the range of liquid breakdown voltage V_{LB} to gaseous one V_{GB}. They were estimated according to empirical formula of breakdown voltage against the gap length for liquid nitrogen[11] and the streamer theory for nitrogen gas[12]. The results are shown in **Table 2**.

Effect of applied voltage Calculated bubble trajectories in the CS-II electrode of g=2mm are illustrated for four voltages in **Fig. 9**. In this case, the bubbles were started from $\theta=\pm2°$, $\pm20°$, $\pm40°$ and $\pm60°$.

At lower applied voltages, all bubbles are directed upward; but with increasing applied voltage, a part of the bubbles leaving from $\theta>0$ starts to move downward and then goes back to the cylinder along the stagnation line. That is, there are minor loop trajectories which start from and return to the cylinder. At higher voltages, some of trajectories touch

Table 2 Estimated values of applicable voltage.

Gap length (mm)	0.5	0.8	2	20	40
V_{GB} (kV)	7.4	11	24	126	175
V_{LB} (kV)	16.7	24.3	50	319	555

the plane electrode and then overshoot when they arrive at the stagnation line.

From examination of calculated bubble trajectories, bubble behavior is categorized into four groups depending on the spatial region in the gap as shown in **Fig. 10**:

A : bubble rises without collision on the plane electrode,

B : bubble rises with collision on the plane electrode,

C : bubble goes down and moves along the stagnation line, and

D : bubble rises and then reaches the stagnation line or cylindrical electrode.

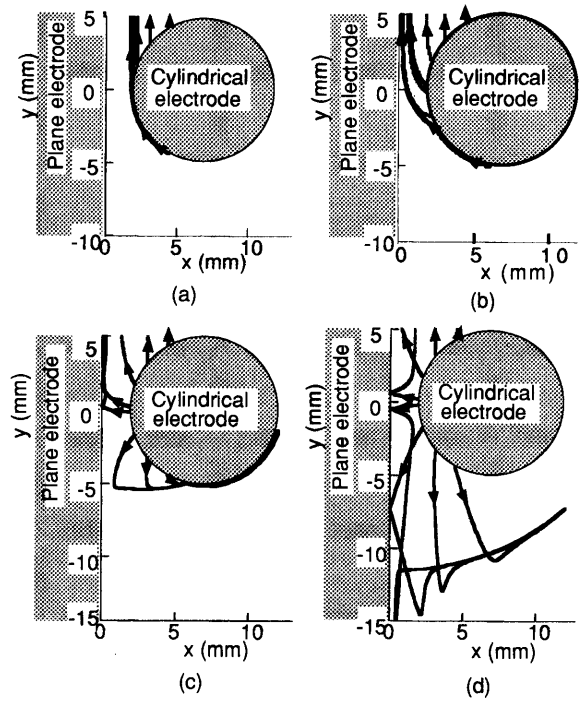

Fig. 9 Calculated bubble trajectories with the CS-II electrode system and g=2mm
(a) V_a=0kV, (b) 6kV, (c) 14kV, (d) 50kV.

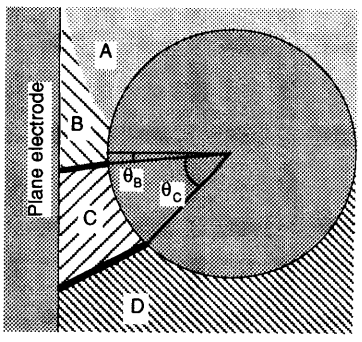

A : rising without collision on the plane electrode
B : rising with collision on the plane electrode
C : going down and leading the stagnation line
D : rising and reach the stagnation line or cylindrical electrode

Fig. 10 Classification of bubble motion and its area.

The angles θ_B and θ_C which are the boundaries among the regions B, C, and D depend on the applied voltage as shown in **Fig. 11**. In the figure, the θ_S on the left and right hands of the minimum in each curve are θ_B and θ_C, respectively. As recognized from a curve for g=2mm, when $\theta_B \fallingdotseq 0$ and $\theta_C > 80°$, the stagnation line, i.e., the boundary between the C and D, is away from the shortest gap region even if the applied voltage is about 40% of the estimated breakdown voltage (50kV) in liquid nitrogen. The minimum point on the curve reveals the voltage V_a and angle θ at the onset of the minor loop trajectory and below it only the region A appears.

Effect of gap length Gap-length dependence of θ_B and θ_C is given also in **Fig. 11**. The V_a and θ at the onset of the minor loop trajectory increase approximately linearly with the gap length of 0 to 5mm at the least. It is concluded from **Fig. 11** that the minor loop will not appear in longer gaps such as g=20 and 40mm since no minimum point appears in the curve. Therefore, no stagnation line appears in long gaps until the breakdown and then no bubble coalescence occurs.

Setting the applied voltage equal to the gaseous breakdown voltage V_{GB} and changing gap length under a constant diameter of cylindrical electrode, the trajectory was calculated as shown in **Fig. 12**. This figure suggests that the characteristic regions disappear in order from the bottom region D to the upper region B with increasing gap length and only the region A remains with a long gap.

Effect of electrode size **Fig. 13** shows the time

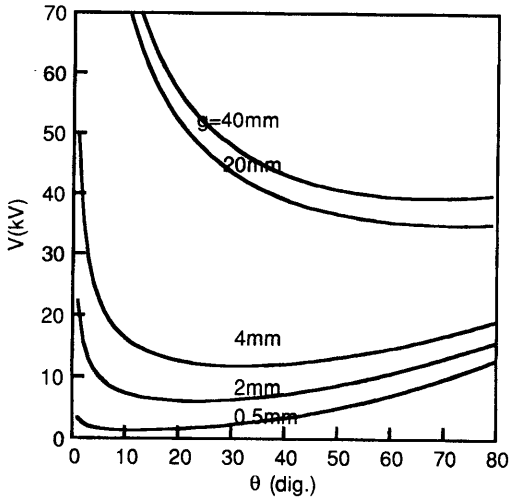

Fig. 11 Applied voltage satisfying $F_{gy}=F_B$.

dependence of traveling speed and time for a bubble released from $\theta=20°$ with the gaps of $g=0.8$mm and 2mm and the same average electric field strength in the gap. Since the bubble velocity is high from the cylindrical electrode to the stagnation line but low along the stagnation line, the bubbles will coalesce near the stagnation line, if the bubbles are supplied continuously from the cylinder.

When one considers two similar electrode systems of 1 and 2 having gap length of g_1 and $g_2=\lambda g_1$ while keeping average electric field constant as the case shown in **Fig. 13**, the gradient forces in the two gaps are related as $F_{g1}(x,y)=\lambda F_{g2}(\lambda x,\lambda y)$. If the buoyancy term is negligible as compared with the other force terms in the motion equation of bubble, the relationship of $V_1(x,y)=V_2(\lambda x,\lambda y)/\lambda$ is valid for the bubble velocity. Therefore, the traveling time on a minor loop trajectory starting from a given θ in the electrode system 2 is λ^2 times longer than that in the system 1. The calculated results of the trajectory show that their patterns are very similar, as expected; but in larger system, the overshoot becomes weaker and the traveling time to the stagnation line is slightly larger than λ^2 times that in the smaller one, as seen in **Fig. 13**. The cause of this disagreement within the above traveling times is due to the fact that the buoyancy term was considered in numerical calculation but neglected in the above discussions.

Effect of bubble radius The calculated trajectories for two bubble radius are illustrated in **Fig. 14**. The larger bubble shows more violent movement than the smaller one. This bubble size effect on the motion can be inferred from the equation of motion of the bubble. Combining Eqns.(3), (4), (5), and (9) and dividing the both sides of the equation by $2\pi a^3$, we obtain

$$\frac{2}{3}\left(\rho_g+\frac{1}{2}\rho_l\right)\frac{d\boldsymbol{V}}{dt}=\frac{\varepsilon_l(\varepsilon_g-\varepsilon_l)}{2\varepsilon_l+\varepsilon_g}\nabla\boldsymbol{E}^2-\frac{2\eta}{a^2}\boldsymbol{V}+\frac{2}{3}(\rho_l-\rho_g)\boldsymbol{G}, \tag{11}$$

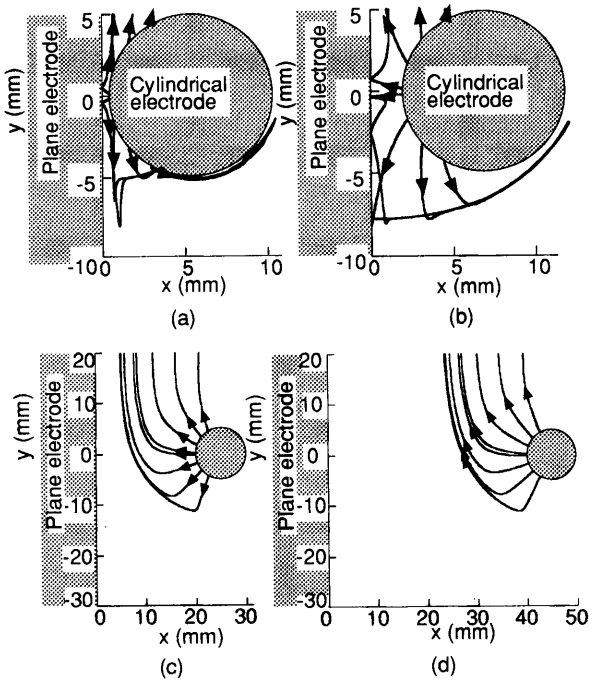

Fig. 12 Effect of gap length on bubble trajectories under $V_a=V_{GB}$ with $a=0.08$mm
(a) $g=0.5$mm, $V_{GB}=7.4$kV, (b) $g=2$mm, $V_{GB}=24$ kV,
(c) $g=20$mm, $V_{GB}=126$kV, (d) $g=40$mm, $V_{GB}=175$ kV,

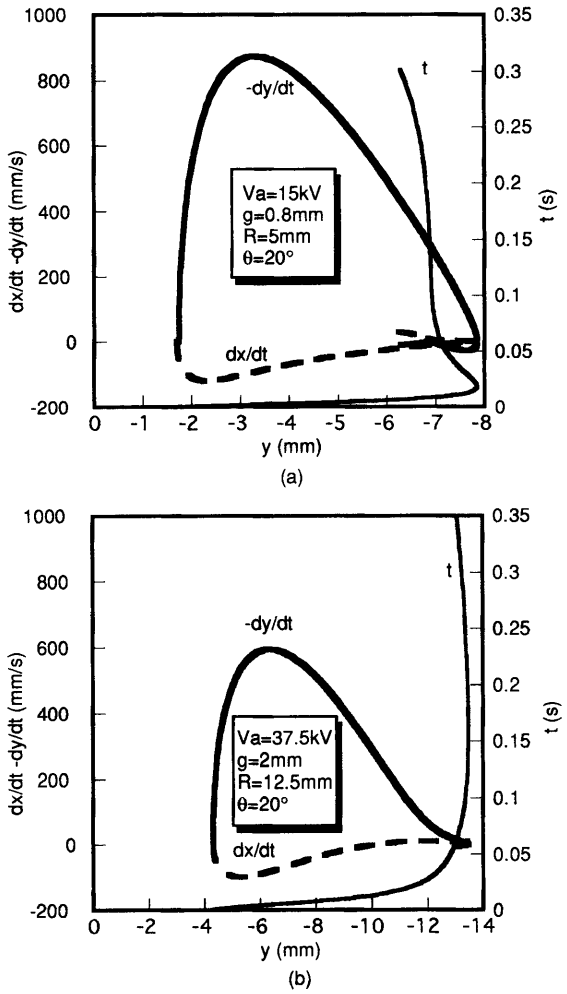

Fig. 13 Traveling time and velocity of bubble started from $\theta=20°$ with $a=0.08$mm as a function of bubble position.
(a) $g=0.08$mm, $R=5$mm, $V_a=15$kV,
(b) $g=2$mm, $R=12.5$mm, $V_a=37.5$kV.

It is now obvious that increasing the bubble radius in Eqn.(11) results in the reduction of effective drag force or increasing of inertia effect.

Effect of electrode arrangement The resultant force acting on the bubble changes also with the electrode arrangement against the direction of gravitational force. Then the bubble trajectory, velocity, and traveling time are calculated for the CS-III and IV with 0.8mm in gap length shown in **Figs. 15** and **16**. As compared with those for the CS-II in **Figs. 9** and **13**(a), the following arrangement effects are recognized.

1) With the CS-III and IV, the y component of velocity is directed always to the outside of gap, in contrast with that of the CS-II case where its direction changes on the way of travel to the outside from the shortest gap region if the applied voltage is so high that the stagnation line is formed.

2) There is no minor loop trajectory in the CS-III and IV.

3) With the CS-II, the bubble velocity can become very low near the stagnation line which appears near $y=-7$mm in **Fig. 13**(a). As stated previously, this slow velocity results in the bubble coalescence along it, if the bubbles are supplied from the cylinder continuously. On the other hand, a high y component of the velocity is maintained in the CS-III and IV, even if the x component is zero, and then a low velocity as in the CS-II electrode system does not appear. Therefore, the bubble coalescence will not occur in these gaps.

4) The time for bubble residence in the gap space with the CS-II is one order longer than those with the CS-III and IV.

Effect of surface roughness of electrode Fin on the cylinder shown in **Fig. 2**(a) enhances electric field in a limited region near it. Then the trajectory of the suspended bubble is very similar to that in the case of smooth cylinder. Moreover, the bubble generated at the bottom of the groove between fins tends to be trapped in the groove since it experiences a gradient force towards the groove bottom. Therefore, the bubble behavior will be affected by surface roughness through the generation process of suspended bubble. This will be described in the next section.

4.3 Behavior of Trapped Bubble in the Groove

The P_s and P_e depend on the θ and the electrode arrangement. Relationship between P_s and P_e around the CC electrode is illustrated in **Fig. 17**; and the estimated distribution of P_s and P_e around the cylinder with $g=0.8$mm is given in **Fig. 18**, where P_e is the value at the point C in **Fig. 3**, $P_s=\rho hG$ and h

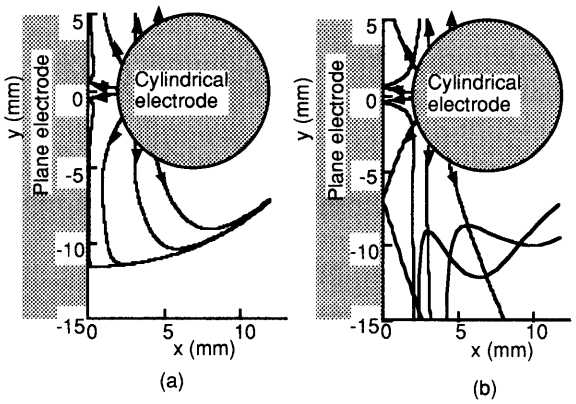

Fig. 14 Effect of bubble size on bubble trajectories under $V_a=50$kV with $g=2$mm
(a) $a=0.04$mm, (b) $a=0.16$mm.

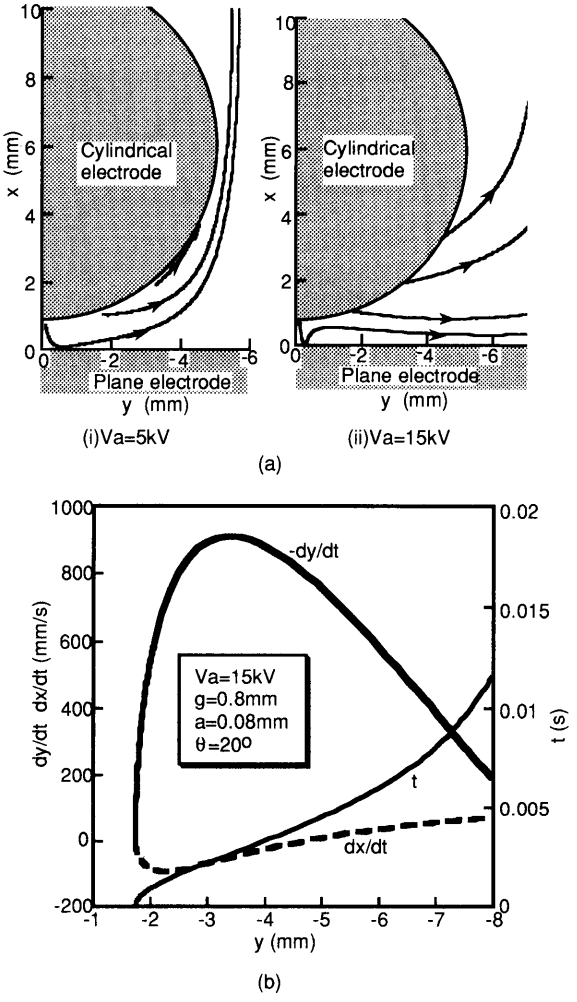

Fig. 15 Bubble trajectories, traveling time and velocity as a function of bubble position with the CS-III electrode system, $g=0.8$mm and $a=0.08$mm
(a) Bubble trajectories,
(b) Traveling time and velocity.

was put as zero at $\theta=0$. Clearly, the P_e is dominant for the behavior of trapped bubble in the groove in any electrode arrangement. It is noted from this figure that a local minimum in P_e+P_s will appear at lower applied voltages only at the CC-IV electrode and will cause the growth of bubble into the gap there. These figures also suggest that the gas around small θ in the groove flows to a large θ region and is released from the groove there as shown in the conceptual diagram, **Fig. 19**.

With the CL electrode, bubble behavior depends on

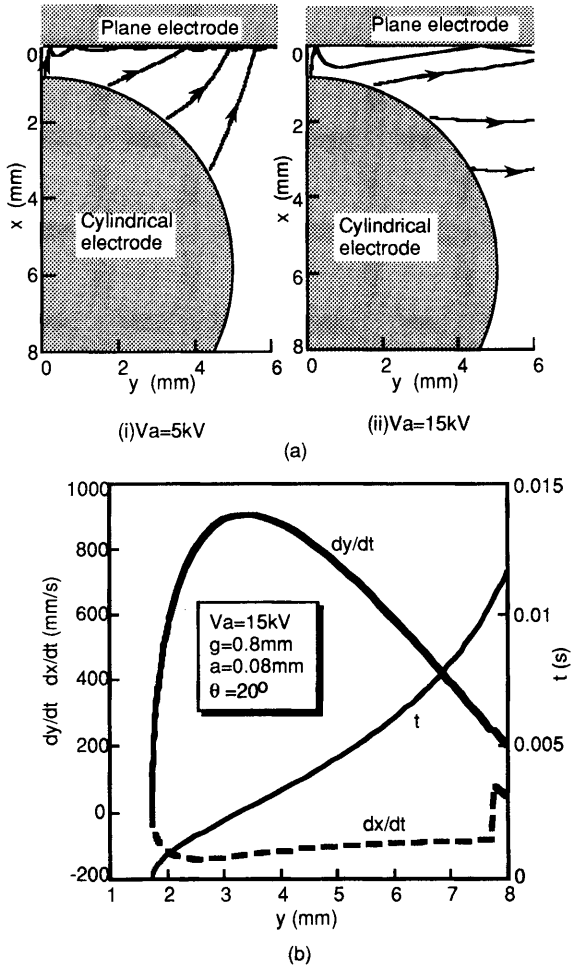

Fig. 16 Bubble trajectories, traveling time and valocity as a function of bubble positions with the CS-IV electrode system, g=0.8mm and a=0.08mm
(a) Bubble trajectories,
(b) Traveling time and velocity.

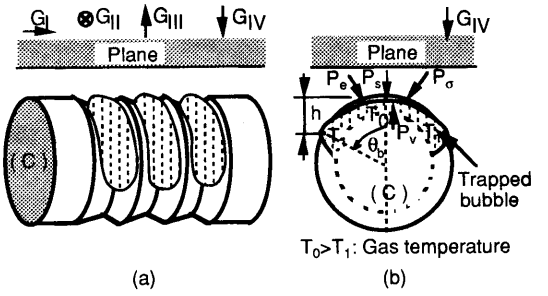

Fig. 17 Relationship between Maxwell stress (P_e) and hydraulic pressure (P_s) with the CC electrode
(a) State of trapped bubble in the groove of CC electrode,
(b) Pressures acting on the surface of trapped bubble.

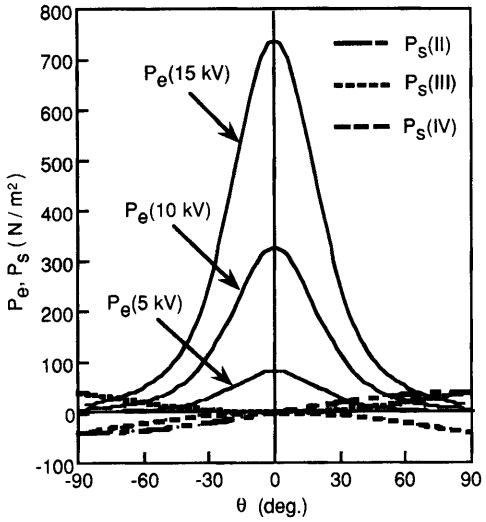

Fig. 18 Distribution of P_e and P_s around the CC electrode with different arrangements with g=0.8mm.

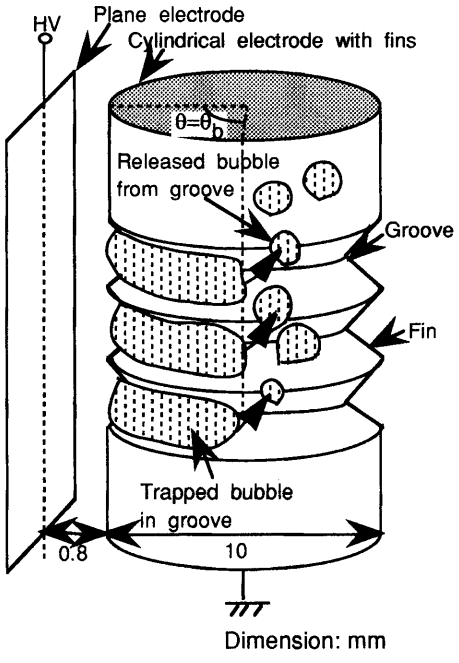

Fig. 19 Estimated conceptual diagram of bubble behavior under high applied voltage with the CC-I electrode system.

the θ, representing the groove position on the cylinder, since the P_e at the representative point C of a groove shown in **Fig. 3** changes with the groove position, θ.

5. Conclusion

Bubble behavior in liquid nitrogen with a cylinder-to-plane gap of 0.5-40mm in length was studied analytically under dc applied voltage. Surface roughness of triangular fins on the cylinder of 10mm in diameter was considered in the analysis. The calculation results of forces acting on a bubble suspended in liquid nitrogen or trapped in groove shows that the electrical forces become predominant as compared with buoyancy, drag force, and non-electrical pressures, even if the applied voltage is much lower than the breakdown voltage of non-uniform field gaps in liquid nitrogen. Bubble trajectory depends on the gap arrangement and gap length. Especially in horizontally arranged electrode system with shorter gap length, the electric field can produce the stagnation region where the electrical gradient force on a suspended bubble balances with the buoyancy and results in the formation of coalesced large bubble. However, in larger gaps the stagnation phenomena of bubbles are estimated not to appear till the breakdown.

With the finned cylinder, pronounced gradient force near the fin tip suppresses the stable growth of bubble there. Moreover, the trapped bubble in a groove between fins tends to flow towards the region of the lower electric field. These suggest that the effect of thermally induced bubble on the breakdown voltage can be minimized if the fins are formed to guide electrically the bubble in the groove from the high external electric field to the lower one.

In this paper, the bubble deformation by electric field has not been dealt with. It had been reported by Garton et al.[13] and its effect on the breakdown voltage will discussed in the Part 2. It is predicted from the above analysis, at least, that deformed bubble in the shortest gap region causes a reduction in breakdown voltage ; but the coalesced bubble hardly causes reduction in breakdown voltage, because it occurs at the place away from the highest field region.

Acknowledgements

This work was supported in part by a Gland-in-Aid for Scientific Research from Ministry of Education, Science and Culture, Japan.

References

1) M. Hara, T. Kaneko and K. Honda : Cryogenics, Vol. 27, pp. 93-101 (1987)
2) M. Hara, K. Honda and T. Kaneko : Cryogenics, Vol. 27, pp. 567-576 (1987)
3) M. Hara, D. J. Kwak and M. Kubuki : Cryogenics, Vol. 29, pp. 895-903 (1989)
4) M. Hara and M. Kubuki : Proc. of IEE, Vol. 137, Pt. A, pp. 209-216 (1990)
5) M. Hara, H. Koishihara and K. Saita : IEEE Trans. on EI, Vol. 26, pp. 685-691 (1991)
6) N. Hayakawa, M. Hirose, H. Goshima, M. Hikita, K. Uchida and H. Okubo : Cryogenics, Vol. 35, pp. 135-142 (1995)
7) M. Hara, Z. C. Wang and H. Saito : Proc. 8th ISH, Yokohama, Japan, Paper No. 93. 01 (1993)
8) M. Hara, Z. C. Wang and H. Saito : IEEE Trans. on DEI, Vol. 1, pp. 709-715 (1994)
9) M. Hara, K. Takano, S. Matsuura and Z. C. Wang : Resarch Reports on Information Science and Electrical Engineering of Kyushu University, Vol. 3, No. 1, pp. 35-43 (1998)
10) H. Lamb : "Hydrodynamics", Dover, New York, Arts. 92 and 337 (1945)
11) M. Hara, T. Kaneko and K. Honda : IEEE Trans. on EI, Vol. 23, pp. 769-778 (1988)
12) A. Petersen : IEEE Trans. on PAS, Vol. 186, pp. 200-206 (1967)
13) C. G. Garton and Z. Krauscki : Proc. Roy. Soc. A280, pp. 211-226 (1964)